Letter Vol. 49, No. 19 / 1 October 2024 / Optics Letters 5587

Observation of multiple topological bound states in the continuum in the photonic bilayer trimer lattice

Weijie Liu,[1] Wenchao Yan,[1,2] Weizhao Cheng,[1] Bin Zhang,[1] Bo Wu,[1] Han Zhu,[1] Lingrui Chu,[1] Yuechen Jia,[1] and Feng Chen[1,*]

[1]School of Physics, State Key Laboratory of Crystal Materials, Shandong University, Jinan 250100, China
[2]yanwenchao@sdu.edu.cn
*drfchen@sdu.edu.cn

Received 5 August 2024; revised 5 September 2024; accepted 7 September 2024; posted 12 September 2024; published 30 September 2024

A topological bound state in the continuum (TBIC) is a novel topological phase that has attracted significant attention. Different from conventional topological insulators (TIs), where boundary states reside within gaps, TBICs can support unconventional boundary states that remain isolated from the surrounding bulk states. In this work, we experimentally demonstrate multiple TBICs in photonic bilayer trimer lattices using femtosecond laser writing technology. By modulating the interlayer coupling between two trimer chains, we observe the emergence of two distinct types of TBICs. Moreover, we experimentally achieve the coexistence of in-gap topological states and TBICs and demonstrate the transformation between them. Our work unveils new insights into the flexible construction of TBICs, and this method can be easily applied to other one-dimensional topological structures, offering promising avenues for further research.

https://doi.org/10.1364/OL.538623

Topological insulators (TIs) have been a subject of extensive research since the discovery of the quantum Hall effect [1]. One of the most intriguing features of TIs is the presence of topologically protected, scatter-free states that propagate along the boundaries of the system, while the bulk remains insulating [2,3]. To date, TIs have been extensively investigated across various physical platforms including photonics [4–10], ultracold atoms [11], electric circuits [12], and so on. In photonics, topological states typically refer to light flow localized at the edge of a photonic lattice without diffraction into the bulk [13–18]. Experimental realizations of TIs in photonics are currently thriving [19–23], and they are increasingly combined with diverse physical concepts such as Floquet engineering [24], nonlinear dynamics [25], and non-Hermitian systems [26]. These combinations create new unique phenomena and bring new possibilities to TIs.

Bound states in the continuum (BICs) refer to the phenomenon where localized state eigenvalues imbed in the continuum of extend states [27]. The combination of TIs and BICs is attractive and natural, as both phenomena involve localized states. This new state, termed topological bound state in the continuum (TBIC), challenges conventional TI understanding where topological edge states typically reside within bandgaps; instead, TBICs exist within the bulk energy band. Recently, TBICs have been demonstrated in some systems including photonics, electric circuits, and acoustics [28–31]. However, the flexible manipulation of TBICs remains challenging. For example, achieving the coexistence or conversion of in-gap topological states and TBICs presents ongoing difficulties.

In this study, we experimentally demonstrate TBICs in bilayer trimer lattices using femtosecond laser writing technology. In the topological phase of such lattice, all topological edge states can be categorized into two types based on their mode distribution characteristics, termed in-phase and out-of-phase edge states. Through modulation of the interlayer coupling, each type of topological states can transition between in-gap states and TBICs. Moreover, under specific interlayer coupling conditions, the structure supports coexisting in-gap topological states and TBICs. This approach provides a straightforward and adaptable method to manipulate both in-gap topological states and TBICs, thereby introducing new degrees of freedom for combining TIs and BICs.

The bilayer trimer lattice consisting of two trimer lattice chains with interlayer coupling t_3 is shown in Fig. 1(a). For each layer, there are intracell coupling t_1 and intercell coupling t_2. The on-site energy of each site is equal. When $t_2 > t_1$, the monolayer trimer lattice is in the topological phase, and there are two topological edge states on each boundary of the lattice [32,33]. The Hamiltonian H of the bilayer trimer lattice in the k space is expressed as $H = \tau_0 \otimes h + t_3 \tau_1 \otimes I$, where τ_0 and τ_1 are the Pauli matrix, and h is the Hamiltonian of a single-layer lattice [31]:

$$h = \begin{pmatrix} 0 & t_1 & t_2 e^{-ik} \\ t_1 & 0 & t_1 \\ t_2 e^{ik} & t_1 & 0 \end{pmatrix}. \tag{1}$$

I is the identity matrix with the same dimension as h. The system satisfies the mirror symmetry $[M_z, H] = 0$, where $M_z = \tau_1 \otimes I$. Thus, the system can be decoupled via similarity transformation [31]. In our model, H can be rewritten as $\tilde{H} = h_1 \oplus h_2$, where $h_1 = h + t_3 I$ and $h_2 = h - t_3 I$. From this perspective, the bilayer trimer lattice is simply the sum of two monolayer trimer lattices with the addition of opposite on-site energy $\pm t_3$, as shown in Fig. 1(a). The on-site energy will induce a global shift in the

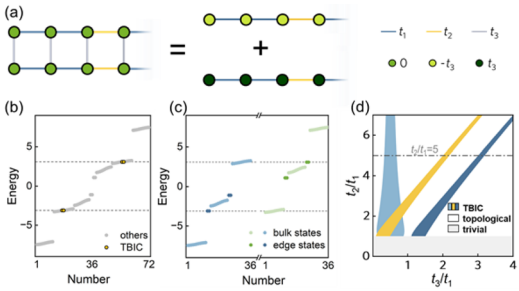

Fig. 1. (a) Schematic of the bilayer trimer lattice and its effective decomposition. According to the theoretical analysis, the change of the on-site energy of the effective one-dimensional lattice is equivalent to the interlayer coupling t_3. (b) Energy spectrum of a finite nontrivial bilayer trimer lattice with 72 sites. Here, $t_1 = 1$, $t_2 = 5$, and $t_3 = 2.1$. Yellow points indicate TBICs and gray points represent other states. Dashed lines denote the value of energy of TBICs. (c) Energy spectrum of the effective two monolayer trimer lattices with different on-site energies. Dark blue and dark green points denote topological states, while light points represent bulk states. Here, $t_1 = 1$, $t_2 = 5$, and $t_3 = 2.1$. (d) Phase diagram of bilayer trimer lattices. The gray area corresponds to the topological trivial phase. The yellow and blue areas correspond to the TBICs.

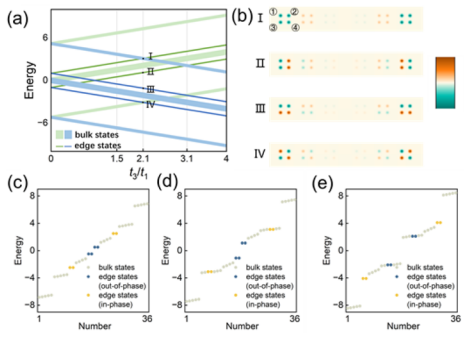

Fig. 2. (a) Eigenvalues of the bilayer trimer lattice as a function of t_3 ($t_2 = 5$). I–IV correspond to the topological states with different energy positions. (b) Mode profiles of each topological state shown as black dots in (a). Here, $t_3 = 2.1$. (c)–(e) Energy spectrums of the structures with $t_3 = 1.5$, 2.1, and 3.1, respectively.

energy spectrum without altering its shape, offering a convenient framework to modulate the energy of topological states by adjusting t_3 in bilayer systems. In order to further illustrate this modulation, we calculate the energy spectrum of a nontrivial bilayer trimer lattice (Fig. 1(b)) and two effective monolayer trimer lattices with opposite on-site energy (Fig. 1(c)). In the following analysis, we set $t_1 = 1$ for convenience. We set $t_2 = 5$ to ensure the system remains in the topological phase. As shown in Fig. 1(b), there is a pair of doubly degenerate TBICs with opposite energy. Figure 1(c) displays the energy spectrum of two effective monolayer trimer lattices. The $\pm t_3$ on-site energies produce overall upward or downward shifts in the spectrum, respectively. With an appropriate t_3, where the energy of topological states in one layer aligns with the bulk of another layer, TBICs emerge. By varying t_2 and t_3, we construct the phase diagram of the bilayer trimer system, as shown in Fig. 1(d). The phase diagram reveals three parameter regions that support TBICs. Based on subsequent analysis, we classify these regions into two types: light blue and dark blue areas represent out-of-phase TBICs, while the yellow area corresponds to the in-phase case.

Next, we investigate the influence of interlayer coupling t_3 in our model ($t_2 = 5$). The energy spectrum of the bilayer trimer lattice as a function of t_3 is depicted in Fig. 2(a). The green and blue segments correspond to energy bands originating from different effective monolayer lattices. Within each segment, broad light areas represent bulk states, while dark lines denote topological edge states. We label the topological states at various energy positions as I–IV.

Figure 2(b) illustrates the mode distributions of these topological states at $t_3 = 2.1$; the four sublattices within the leftmost unit cell are labeled 1–4, respectively. The robustness of topological edge states is protected by inversion symmetry, consistent with a single-layer trimer lattice [32,33]. Modifying t_3 can adjust the degree to which energy penetrates into the bulk, but will not change the phase difference between sites. We can observe that as t_3 varies, eigenvalues are always symmetric at $E = 0$, and topological states I and IV have opposite eigenvalues, so topological states I and IV consistently exhibit TBICs or not. Topological states II and III exhibit same behaviors. Interestingly, for topological states in II and III, sites 1 and 4 consistently maintain the opposite phase. Conversely, for states I and IV, sites 1 and 4 consistently maintain the same phase. Therefore, we classify topological states II and III as out-of-phase topological edge states, and those in I and IV as in-phase topological edge states. For the out-of-phase topological edge states, TBICs appear in two parameter ranges: 0.3–0.7 and 3.0–3.2, which is consistent with Fig. 1(d). When t_3 ranges from 2.0 to 2.2, the in-phase topological states transition into TBICs. We choose three specific values of t_3: 1.5, 2.1, and 3.1 and present the corresponding energy spectrums in Figs. 2(c)–2(e). At $t_3 = 1.5$, all topological states remain the in-gap states. At $t_3 = 2.1$, the in-phase topological states exhibit TBICs, while the out-of-phase topological states remain in-gap. Conversely, at $t_3 = 3.1$, out-of-phase topological states exhibit TBICs, while the in-phase topological states are in-gap.

To experimentally demonstrate TBICs, we fabricated the bilayer trimer lattices using femtosecond laser writing technology [34–37]. The borosilicate glass (Eagle XG) sample is mounted on a 3D x–y–z translation stage. A femtosecond laser (Femto YL-25, YSL Photonics) with a wavelength of 1030 nm, a repletion rate of 2.5 MHz, and a pulse duration of 400 fs is used. A microscope objective focuses the laser into the glass at the depth of 230 μm. The array is oriented along the z direction and arranged in the x–y plane. The structure is illustrated in Fig. 3(a). Figure 3(b) displays the microscope image of the input face of the structure. The evolution of light in the waveguide array follows the Schrödinger-type function:

$$i\frac{\partial\psi(x,y;z)}{\partial z} = -\left(\frac{\nabla_\perp^2}{2k} + \frac{\Delta n(x,y;z)k}{n_0}\right)\psi(x,y;z) \equiv H\psi(x,y;z), \tag{2}$$

where ψ is the electric field envelope of the light, $k = 2\pi/\lambda$ corresponds to the wavenumber, $\Delta n(x, y; z)$ is the index modulation, and n_0 is the substrate refractive index. The relation between the coupling coefficient of two adjacent waveguides and the spacing d follows the equation $t = Ae^{-\gamma d}$. In this work, the light with a wavelength of 532 nm is injected into the waveguides, where $A = 3903\ \mathrm{m}^{-1}$ and $\gamma = 0.256$. t_1, t_2, and t_3 correspond to d_1, d_2, and d_3 in the structure, respectively (Fig. 3(b)). We set $t_1 = 50\ \mathrm{m}^{-1}$ corresponding to d_1 of 17 μm. Other spacing parameters of the structure can be adjusted via the coupling ratio. We set $t_2 = 5t_1$

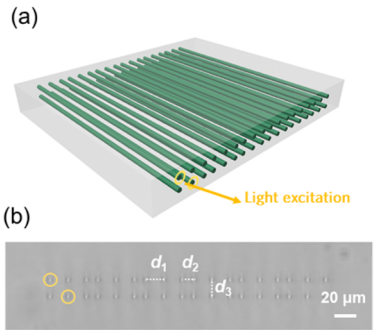

Fig. 3. (a) Schematic of the photonic lattice fabricated by femtosecond laser writing technology. Yellow circles are the sites where the light is injected to the structure. (b) Optical micrograph of the input facet of the waveguide lattice. We set $d_1 = 17$ μm and $d_2 = 10.7$ μm for all lattices. The length of d_3 varies with t_3 and this structure corresponds to $t_3 = 1.5t_1$ case where $d_3 = 15.4$ μm.

for all experimental structures and $t_3 = 1.5t_1$, $2.1t_1$, and $3.1t_1$ corresponding to $d_3 = 15.4$ μm, 14.1 μm, and 12.6 μm, respectively. The propagation length of the structure is 25 mm to ensure adequate light evaluation. It is noteworthy that when $t_3 < t_1$, there is another out-of-phase TBIC area, as shown in Fig. 1(d). However, in this case, due to the weak interlayer coupling, significant interlayer interactions require a very long propagation length. To distinguish between in-phase and out-phase topological states experimentally, the light is injected into sites 1 and 4 of the lattices with same intensity and tunable phases by a spatial light modulator, as depicted by yellow circles in Fig. 3(a). When the two light beams are out-of-phase, topological states II and III are excited, and when two lights are in-phase, topological states I and IV are excited. The light field distribution at the output of the lattice is captured by a charge-coupled device.

Experimental and simulated results are demonstrated in Fig. 4. First, we set $d_3 = 15.4$ μm and Figs. 4(a)–4(b) depict the results when the injected light beams are in-phase. After propagating 25 mm, the light beams localize predominantly at the left boundary of the lattice, and modulating d_3 or employing different exciting methods, as illustrated below, still maintains this locality, indicating the excited states are topological boundary states. Due to the ΔE between topological states I and IV, a light beating phenomenon occurs during light propagation, where the beating length l is determined by $l = \pi/\Delta E$, with ΔE representing the energy difference between two edge states [38]. The light beams oscillate between sites 1 and 4 and sites 2 and 3 (Fig. 4(b)). In this case, $l = 26.5$ mm and most of the light intensity transforms from initial sites 1 and 4 to sites 2 and 3 at the output of the lattice. Simulated results under the same parameters are obtained using the beam propagation method by Rsoft and the simulated results agree well with the experimental results. Figures 4(c)–4(d) show the results when the injected light beams are out-of-phase. In this case, topological states II and III are excited simultaneously. Due to a smaller ΔE between states II and III compared to states I and IV within the same structure, there is a larger beating length and resulting in a distinct light propagating behavior. l is 108 mm and at the output of the lattice, the majority of light intensity is still in the initial sites. Under this structure, all the topological states reside within the bandgap, allowing both in-phase and out-of-phase excitations to obtain in-gap topological states. Meanwhile, Figs. 4(e)–4(h) show the results for $d_3 = 14.1$ μm. Compared to the first structure, the t_3 of this lattice is larger, inducing a greater ΔE between states I and IV, which leads to a shorter l. The ΔE between states II and III shows the same trend. Here, l is 19.5 mm for in-phase excitation and 43.4 mm for out-of-phase excitation. Notably, states I and IV are in the bulk in this case. Thus, we experimentally demonstrate the TBICs by in-phase excitation. Meanwhile, the states by out-of-phase excitation, corresponding to states II and III, are still in the bandgap. Thus, we demonstrate the coexistence of in-gap topological states and TBICs in the same structure. For $d_3 = 12.6$ μm, the interlayer coupling t_3 is larger and l is shorter. l is 13.4 mm for in-phase excitation and 21 mm for out-of-phase excitation (Figs. 4(i)–4(l)). As the energy of states II and III are in the bulk while states I and IV are in the bandgap, we experimentally realized out-of-phase TBICs and in-phase in-gap topological states, and by modulating interlayer spacing d_3, for each type of topological states, such as in-phase states, we achieve the transformation from the in-gap topological states ($d_3 = 15.4$ μm, 12.6 μm) to TBICs ($d_3 = 14.1$ μm).

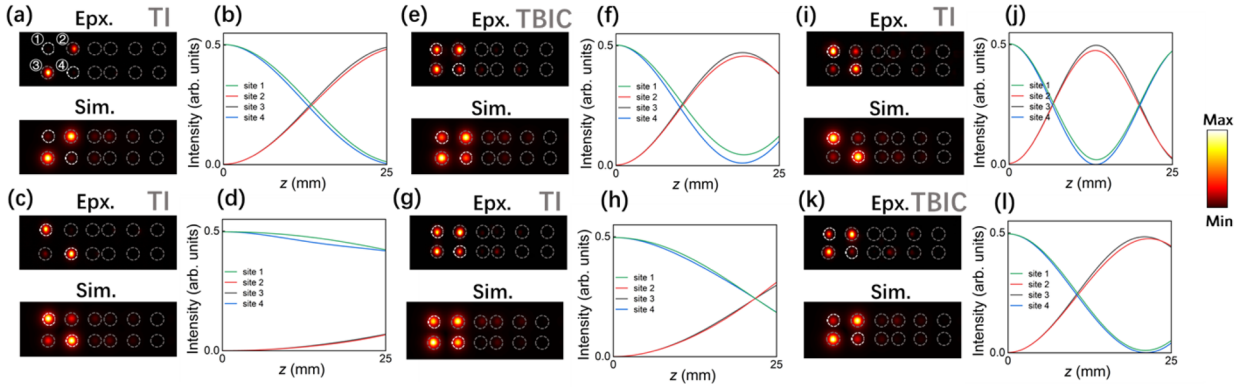

Fig. 4. (a) Experimental and simulated results of the output intensity pattern of the lattice with $d_3 = 15.4$ μm ($t_3 = 1.5t_1$) after propagating 25 mm. The white circles mark the excited sites and the gray circles mark the other sites. The excited light beams at two sites are in-phase. (b) Simulated propagation dynamics with the same structural parameters and exciting way of (a). The light intensities of sites 1–4 are presented. (c) Experimental and simulated results of the output intensity pattern of the lattice with $d_3 = 15.4$ μm ($t_3 = 1.5t_1$). The excited light beams at two sites are out-of-phase. (d) Simulated propagation dynamics with the same structural parameters and exciting way of (c). (e)–(h) Experimental and simulated results with $d_3 = 14.1$ μm ($t_3 = 2.1t_1$). (e)–(f) are with in-phase excitation and TBICs are realized in this case. (g)–(h) are with out-of-phase excitation. (i)–(l) Experimental and simulated results with $d_3 = 12.6$ μm ($t_3 = 3.1t_1$). (i)–(j) are with in-phase excitation. (k)–(l) are with out-of-phase excitation and TBICs are realized in this case.

In conclusion, we have conducted a detailed investigation into the origin of TBICs in bilayer trimer lattices and introduced a straightforward method to control TBIC within the system. We experimentally demonstrated the existence of TBICs in the lattices. By finely tuning the interlayer coupling, the independent emergence and disappearance of in-phase and out-of-phase TBICs are observed. In cases where the system supports both in-gap topological states and TBICs, each type of state is selectively excited independently. Our work provides a new insight into understanding the relation between TIs and BICs.

Funding. Natural Science Foundation of Shandong Province (ZR2021ZD02, ZR2023QA125); National Natural Science Foundation of China (12174222, 12304364); Taishan Scholar Foundation of Shandong Province (tspd20210303).

Disclosures. The authors declare no conflicts of interest.

Data availability. Data underlying the results presented in this paper are not publicly available at this time but may be obtained from the authors upon reasonable request.

REFERENCES

1. K. v. Klitzing, G. Dorda, and M. Pepper, Phys. Rev. Lett. **45**, 494 (1980).
2. D. J. Thouless, M. Kohmoto, M. P. Nightingale, *et al.*, Phys. Rev. Lett. **49**, 405 (1982).
3. X. L. Qi and S. C. Zhang, Rev. Mod. Phys. **83**, 1057 (2011).
4. J. Noh, W. A. Benalcazar, S. Huang, *et al.*, Nat. Photonics **12**, 408 (2018).
5. A. Fritzsche, T. Biesenthal, L. J. Maczewsky, *et al.*, Nat. Mater. **23**, 377 (2024).
6. Y. Sun, X. Hou, T. Wan, *et al.*, Phys. Rev. Lett. **132**, 063804 (2024).
7. Q. Cheng, H. Wang, Y. Ke, *et al.*, Nat. Commun. **13**, 249 (2022).
8. Y. V. Kartashov, A. A. Arkhipova, S. A. Zhuravitskii, *et al.*, Phys. Rev. Lett. **128**, 093901 (2022).
9. G. G. Pyrialakos, J. Beck, M. Heinrich, *et al.*, Nat. Mater. **21**, 634 (2022).
10. E. Lustig, L. J. Maczewsky, J. Beck, *et al.*, Nature **609**, 931 (2022).
11. N. Goldman, J. C. Budich, and P. Zoller, Nat. Phys. **12**, 639 (2016).
12. Z. Zhang, B. Wu, J. Song, *et al.*, Phys. Rev. B **100**, 184202 (2019).
13. W. Liu, C. Wu, Y. Jia, *et al.*, Phys. Rev. A **105**, L061502 (2022).
14. G. Cáceres-Aravena, B. Real, D. Guzmán-Silva, *et al.*, Phys. Rev. Res. **4**, 013185 (2022).
15. S. Mukherjee and M. C. Rechtsman, Phys. Rev. X **11**, 041057 (2021).
16. N. K. Efremidis, Phys. Rev. A **104**, 053531 (2021).
17. W. Zhang, D. Zou, Q. Pei, *et al.*, Phys. Rev. Lett. **126**, 146802 (2021).
18. W. Yan, W. Cheng, W. Liu, *et al.*, Opt. Lett. **48**, 1802 (2023).
19. Y. Chang, J. Xue, Y. Han, *et al.*, Phys. Rev. A **108**, 062409 (2023).
20. Z. Yang, E. Lustig, Y. Lumer, *et al.*, Light: Sci. Appl. **9**, 128 (2020).
21. L. J. Maczewsky, J. M. Zeuner, S. Nolte, *et al.*, Nat. Commun. **8**, 13756 (2017).
22. L. Liu, Y. Wang, F. Zheng, *et al.*, Opt. Lett. **47**, 2634 (2022).
23. Y. Yuan, L. Liu, Y. Zhou, *et al.*, Opt. Lett. **49**, 4449 (2024).
24. M. C. Rechtsman, J. M. Zeuner, Y. Plotnik, *et al.*, Nature **496**, 196 (2013).
25. D. Leykam and Y. D. Chong, Phys. Rev. Lett. **117**, 143901 (2016).
26. S. Weimann, M. Kremer, Y. Plotnik, *et al.*, Nat. Mater. **16**, 433 (2017).
27. Y. Plotnik, O. Peleg, F. Dreisow, *et al.*, Phys. Rev. Lett. **107**, 183901 (2011).
28. A. Cerjan, M. Jurgensen, W. A. Benalcazar, *et al.*, Phys. Rev. Lett. **125**, 213901 (2020).
29. Z. Li, J. Wu, X. Huang, *et al.*, Appl. Phys. Lett. **116**, 263501 (2020).
30. L. Liu, T. Li, Q. Zhang, *et al.*, Phys. Rev. Lett. **130**, 106301 (2023).
31. Y. X. Xiao, G. Ma, Z. Q. Zhang, *et al.*, Phys. Rev. Lett. **118**, 166803 (2017).
32. V. M. Martinez Alvarez and M. D. Coutinho-Filho, Phys. Rev. A **99**, 013833 (2019).
33. Y. Zhang, B. Ren, Y. Li, *et al.*, Opt. Express **29**, 42827 (2021).
34. W. Liu, Q. Liu, X. Ni, *et al.*, Nat. Commun. **15**, 946 (2024).
35. Q. Liu, W. Liu, K. Ziegler, *et al.*, Phys. Rev. Lett. **130**, 103801 (2023).
36. D. Tan, X. Sun, Q. Wang, *et al.*, Opt. Lett. **45**, 3941 (2020).
37. H. Hanafi, P. Menz, and C. Denz, Adv. Opt. Mater. **10**, 2102523 (2022).
38. M. Kremer, I. Petrides, E. Meyer, *et al.*, Nat. Commun. **11**, 907 (2020).